MOLECULAR BIOLOGY

Enzymatic transfer of acetate on histones from lysine reservoir sites to lysine activating sites

Mariel Mendoza[1,2]†, Gabor Egervari[1,3]*†, Simone Sidoli[1,2]‡, Greg Donahue[1,3], Desi C. Alexander[1,3], Payel Sen[1,3]§, Benjamin A. Garcia[1,2]*||, Shelley L. Berger[1,3]*

Histone acetylation is governed by nuclear acetyl-CoA pools generated, in part, from local acetate by metabolic enzyme acetyl-CoA synthetase 2 (ACSS2). We hypothesize that during gene activation, a local transfer of intact acetate occurs via sequential action of epigenetic and metabolic enzymes. Using stable isotope labeling, we detect transfer between histone acetylation sites both in vitro using purified mammalian enzymes and in vivo using quiescence exit in *Saccharomyces cerevisiae* as a change-of-state model. We show that Acs2, the yeast ortholog of ACSS2, is recruited to chromatin during quiescence exit and observe dynamic histone acetylation changes proximal to Acs2 peaks. We find that Acs2 is preferentially associated with the most up-regulated genes, suggesting that acetyl group transfer plays an important role in gene activation. Overall, our data reveal direct transfer of acetate between histone lysine residues to facilitate rapid transcriptional induction, an exchange that may be critical during changes in nutrient availability.

INTRODUCTION

While long thought to be relegated to separate cellular compartments, recent findings highlight connections between metabolism and gene expression through the presence of metabolic enzymes and metabolites that shuttle between the cytoplasm and the nucleus (*1*–*5*). Key metabolites modulate gene expression through posttranslational modifications of histone tails. For example, *S*-adenosyl methionine and acetyl–coenzyme A (CoA) contribute methyl and acetyl groups for deposition on histone proteins through methyltransferase and acetyltransferase enzymes, respectively (*6*, *7*). Nuclear acetyl-CoA pools are affected by dynamic activities of histone acetyltransferases (HATs) and histone deacetylases (HDACs) (*6*), as well as by increased nuclear localization of various metabolic enzymes that contribute to acetyl-CoA production (*3*, *8*). Acetyl-CoA synthetase 2 (ACSS2), for example, translocates to the nucleus and converts acetate into acetyl-CoA that can be used for histone acetylation and can lead to rapid gene activation, which is vital when cells are under metabolic stress (*3*, *4*, *9*).

Metabolites retained in chromatin not only function as protein modifications for gene regulation but also have been proposed to act as storage for utilization during low nutrient availability. Histones are the most abundant class of proteins in the nucleus and thus have the capacity to store substantial amounts of metabolites. In human cells, recent estimates suggest that ~3 μM acetate could be produced from deacetylation of ~0.1% of histone lysine residues for generation of acetyl-CoA (*10*). This highlights the substantial amount of acetate that has the potential to be released from histones, which can then be directly converted to acetyl-CoA via nuclear ACSS2. Recent studies have proposed that acetate released from histones can be recycled to maintain histone acetylation, especially during metabolic stress such as glucose or oxygen deprivation (*11*–*14*). ACSS2 has been proposed to recapture acetate released by HDACs and to provide a local pool of acetyl-CoA for histone acetylation (*11*, *14*). Overall, these findings suggest that there may be recycling of acetate from stored histone acetylation to new sites of gene-activating histone acetylation sites, and further suggest that this recycling requires direct collaboration of HDACs, ACSS2, and HATs. While this model potentially accounts for dynamic and rapid changes in histone acetylation for gene activation, direct transfer of intact acetate between histone lysine residues remains to be demonstrated.

Here, we use proteomic and genomic approaches to query whether intact acetate can be directly transferred between histone residues in vitro and whether local transfer of intact acetyl groups can be detected in vivo using a change-of-state model in yeast. We interrogate whether ACSS2 can facilitate the local transfer of acetyl groups. Our results point to direct transfer of intact acetate that is mediated by ACSS2, underscoring a critical function of acetate transfer in using local and nuclear acetate pools for histone acetylation and rapid transcriptional activation.

RESULTS

In vitro assays demonstrate direct transfer of intact acetate between histone acetyl-lysine residues

We tested whether histone acetyl transfer can occur in vitro in a reconstituted system with purified enzymes. We used a synthetic histone peptide as substrate, spanning the first 42 amino acids of the histone H3.1 tail, wherein an acetylation site—K23 acetylation (H3K23ac) as the most central site within the peptide—was labeled via "heavy" acetylation with deuterium (Fig. 1A). This leads to a molecular weight increase of 3 Da for the fully deuterated acetyl group, which allows tracking the fate of the intact acetyl group enzymatically released from the labeled acetylation site. We incubated the synthetic peptide in the presence of an HDAC and ACSS2.

[1]Epigenetics Institute, Perelman School of Medicine, University of Pennsylvania, Philadelphia, PA, USA. [2]Department of Biochemistry and Biophysics, University of Pennsylvania, Philadelphia, PA, USA. [3]Department of Cell and Developmental Biology, Perelman School of Medicine, University of Pennsylvania, Philadelphia, PA, USA.
*Corresponding author. Email: egervari@pennmedicine.upenn.edu (G.E.); bagarcia@wustl.edu (B.A.G.); bergers@pennmedicine.upenn.edu (S.L.B.)
†These authors contributed equally to this work.
‡Present address: Department of Biochemistry, Albert Einstein College of Medicine, New York, NY, USA.
§Present address: Laboratory of Genetics and Genomics, National Institute on Aging, Baltimore, MD, USA.
||Present address: Department of Biochemistry and Molecular Biophysics, Washington University School of Medicine, St. Louis, MO, USA.

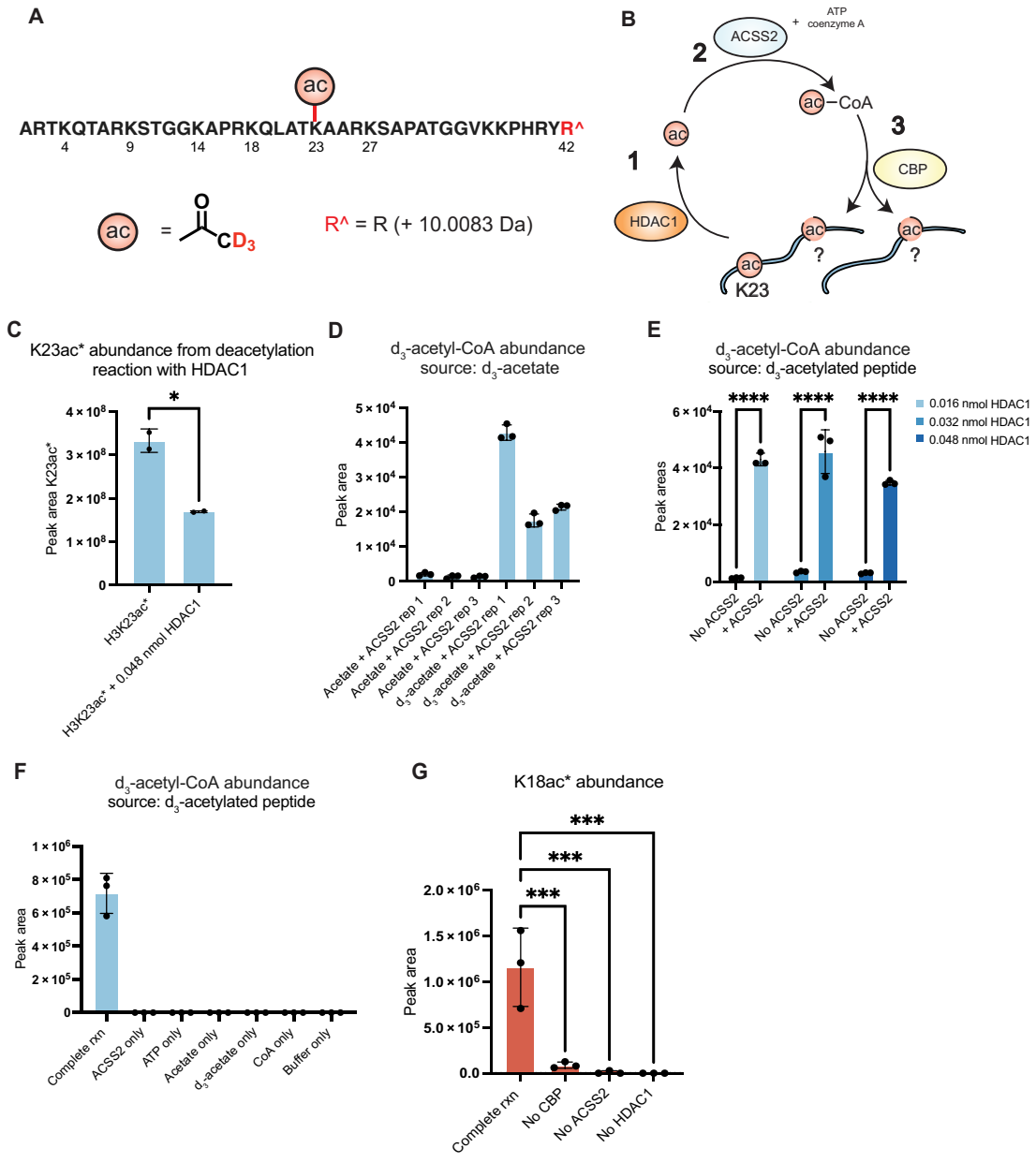

Fig. 1. ACSS2 mediates local transfer of acetyl groups between histone lysine residues. (**A**) Synthetic peptides spanning the first 42 amino acids of the histone H3 tail were designed for the in vitro assays. The acetyl group on K23 is deuterated (K23ac*) to track the transfer. The last amino acid in the peptide was heavy-labeled (^{13}C, ^{15}N) to discriminate the synthetic peptide from peptides derived from endogenous histones. (**B**) Schematic for the in vitro assays performed for acetyl-CoA analysis. The numbers illustrate the three consecutive reactions that must occur for acetyl-transfer to take place. (**C**) Deacetylation reaction with HDAC1 and synthetic histone peptide. *P* value ($P = 0.0136$) was calculated using unpaired *t* test. (**D**) ACSS2 can generate deuterated acetyl-CoA (d_3-acetyl-CoA) from deuterated acetate (d_3-acetate), showing that step 2 from the schematic in Fig. 2B can take place. Bar graphs represent mean ± SD; $n = 3$ per group. (**E**) ACSS2 can generate d_3-acetyl-CoA from K23ac* as the source for acetate. Bar graphs represent mean ± SD; $n = 3$ per group. *P* values were calculated using two-way ANOVA with Sidak's multiple comparisons test. ****$P_{adj} < 0.0001$. (**F**) d_3-acetyl-CoA is produced from deacetylation of histone peptides, showing that steps 1 and 2 from the schematic in (B) can take place. Complete rxn indicates that all three enzymes (HDAC1, ACSS2, and CBP) are present. Bar graphs represent mean and SD; $n = 3$ per group. (**G**) H3K18ac** is observed when all three necessary enzymes were added in the in vitro reactions. Bar graphs represent mean and SD; $n = 3$ per group. *P* values were calculated using one-way ANOVA with Dunnett's multiple comparisons test. ***$P_{adj} < 0.001$.

Cofactors, adenosine triphosphate (ATP), and CoA were included to resemble an environment of high local concentration of these components, which are necessary for the ACSS2 reaction. For full acetyl-CoA production from enzyme action, we expected the following: (i) removal of labeled intact acetyl group (ac*) by an HDAC to produce fully labeled acetate and (ii) conversion of the labeled intact acetate by ACSS2 to generate labeled acetyl-CoA (Fig. 1B).

We first carried out several control reactions. For deacetylation (see step 1, schematic Fig. 1B), we used HDAC1 because it is an

abundant enzyme in the nucleus involved in transcription (*15*, *16*) and because it readily deacetylates histones H3 and H4 (*17*). We found that HDAC1 efficiently deacetylated the synthetic histone peptide in vitro to produce fully labeled acetate (Fig. 1C). To assess whether ACSS2 can produce acetyl-CoA from histone deacetylation, we used a targeted mass spectrometry (MS)–based approach using selected reaction monitoring (SRM) to detect fragment ions specific to fully labeled acetyl-CoA (*18*). We first confirmed that ACSS2 can use labeled acetate to produce labeled acetyl-CoA in vitro (Fig. 1D), thus demonstrating step 2 from schematic Fig. 1B.

We next put steps 1 + 2 together (schematic Fig. 1B), testing whether the synthetic histone peptide can be used by ACSS2 as a source of acetate to generate acetyl-CoA. We incubated the H3K23ac* peptide with HDAC1 and ACSS2 (2 hours) and detected fully labeled acetyl-CoA generated from the acetate released from deacetylation of the histone peptide [$P < 0.0001$, two-way analysis of variance (ANOVA)] (Fig. 1E). In addition, we demonstrated that both enzymes (and cofactors) were necessary for this production of acetyl-CoA via individual enzyme (and cofactor) dropout (Fig. 1F). Overall, these results show that an acetylated histone peptide acts as a source for acetyl-CoA production via sequential action of HDAC1 and ACSS2, via transfer of intact acetate.

We further dissected the role of ACSS2 in dynamic local histone acetylation, testing whether the fully labeled acetyl-CoA produced by ACSS2 can be re-incorporated into the histone peptide (step 3, schematic Fig. 1B). As HAT, we used CREB binding protein (CBP) based on its role in gene activation and its association with ACSS2 in vivo (*12*). We applied two different methods to identify and quantify acetylation. First, we used parallel reaction monitoring (PRM) to specifically target the synthetic peptide and its various acetylated forms (*19*). This method attained sufficient fragmentation of the synthetic peptide, which was crucial in identifying different acetylation sites on the peptide (fig. S1A).

We then performed in vitro reactions with the H3K23ac* peptide and, when all three enzymes (HDAC1, ACSS2, and CBP) were present, we identified the presence of a one newly labeled peptide—H3K18ac*—that was fully deuterated and thus resulting from complete transfer of intact acetate (fig. S1, B and C). To verify the identity of the newly labeled peptide, we used a second method to quantify H3K18ac*, by digesting the synthetic peptide after the reaction followed by analysis using data-independent acquisition (DIA), which is a method routinely used in quantifying histone post-translational modifications (PTMs) from cells and tissues (fig. S2A) (*20*–*23*). ACSS2 was crucial in mediating the transfer, as there was a significant decrease in H3K18ac* when ACSS2 was not present ($P < 0.001$, one-way ANOVA) (Fig. 1G and fig. S2, B and C). Further, HDAC1 and CBP were also critical in the transfer (Fig. 1G and fig. S2C).

These results show that in a purely in vitro system with HDAC1, ACSS2, and CBP HAT, intact acetyl groups are transferred from one histone lysine residue to another. While the reason and mechanism for transfer uniquely to H3K18ac is not clear, the detection of acetyl transfer in vitro supports the hypothesis that ACSS2, collaborating with HDAC and HAT enzymes, can facilitate local transfer of acetyl groups between histone sites.

Acetyl groups are transferred between histone residues during yeast quiescence exit

To investigate acetyl group transfer in vivo, we used a well-characterized change-of-state model in *Saccharomyces cerevisiae*, in which cells exit quiescence and enter exponential growth (*24*). Quiescence exit is accompanied by exceedingly rapid transcriptional changes resulting in increased expression of growth genes (~500 genes) and decreased expression of stress genes (~100 genes) (*24*, *25*). We and others have shown that exit from quiescence is characterized by dynamic changes of histone acetylation (*24*, *25*) [but not of histone methylation (*25*)]: Acetylation is low during quiescence and increases during quiescence exit specifically at growth genes (*25*). On the basis of our in vitro results, we hypothesized that direct transfer of acetyl groups between histone lysine residues could contribute to the remarkably rapid and dynamic histone acetylation changes during quiescence exit to support transcriptional activation.

To test this, yeast cultures were induced to enter quiescence by replacing glucose-rich medium with distilled water for 7 days (*24*, *25*). To trace acetyl groups, water was supplemented with heavy-labeled d_3-acetate (Fig. 2A). Subsequently, cells were washed to remove residual heavy acetate, and quiescence exit and proliferation were induced by resupplying glucose and other nutrients. To ensure that the washing step was sufficient to eliminate extracellular d_3-acetate that had not been internalized, aliquots of the medium were sampled before and after washing, and d_3-acetate levels were measured by MS. We observed a significant decrease in d_3-acetate ($P < 0.0001$, unpaired *t* test) after the wash, indicating that the washing step was efficient in removing excess extracellular d_3-acetate (fig. S3A). Heavy labeling of histone acetylation was then measured using peptide-centric MS (*22*, *23*). We carried out three biological replicate experiments. We note that labeling was variable in these experiments, specifically at the lower abundance histone acetylation sites H3K9 and H3K27. This was due to the difficulty of the data analysis when analyzing labeling rates of lowly abundant modifications. Also, several histone peptides are isobaric (i.e., H3K9ac/K14ac), so quantification of the heavy labeling occurs at the fragment ion level, which are at lower intensity than the intact mass of the peptides. As a result, extracting the signal of the fragment ions containing the heavy labeling remains challenging, which resulted in variability of labeling rates.

Nevertheless, we observed an intriguing pattern of deuterated acetate incorporation on histone H3 in this model. Heavy labeling at K14ac, K18ac, and K23ac was more enriched in quiescent cells compared to labeling of K9ac and K27ac ($P < 0.001$, two-way ANOVA) (Fig. 2B). These results indicate that fully labeled acetate was preferentially stored on specific histone H3 lysine residues in quiescent yeast cells. Notably, during quiescence exit, heavy label incorporation increased at K9ac and K27ac, while the heavy labeling of K14ac, K18ac, and K23ac decreased (Fig. 2B). These distinct labeling patterns (and the fact that d_3-acetate was washed out from quiescent cultures before re-feeding with glucose) suggest that heavy labels deposited on specific lysine residues during quiescence were transferred onto other lysines during quiescence exit.

For histone H4, we were able to accurately quantify only H4K16ac*, as acetylation at other lysine residues (K5/8/12) is not distinguishable—these sites have the same precursor mass/charge ratio (m/z), and they also co-elute by reversed-phase chromatography (*26*, *27*). The highest enrichment of heavy labeling at H4K16ac occurred during quiescence, and heavy label was decreased during quiescence exit (Fig. 2C). These data suggest that, similarly to H3K14ac, K18ac, and K23ac, H4K16ac might be an important site of acetate storage in quiescent yeast cells, from which acetyl groups can be transferred onto other residues as transcriptional demand increases.

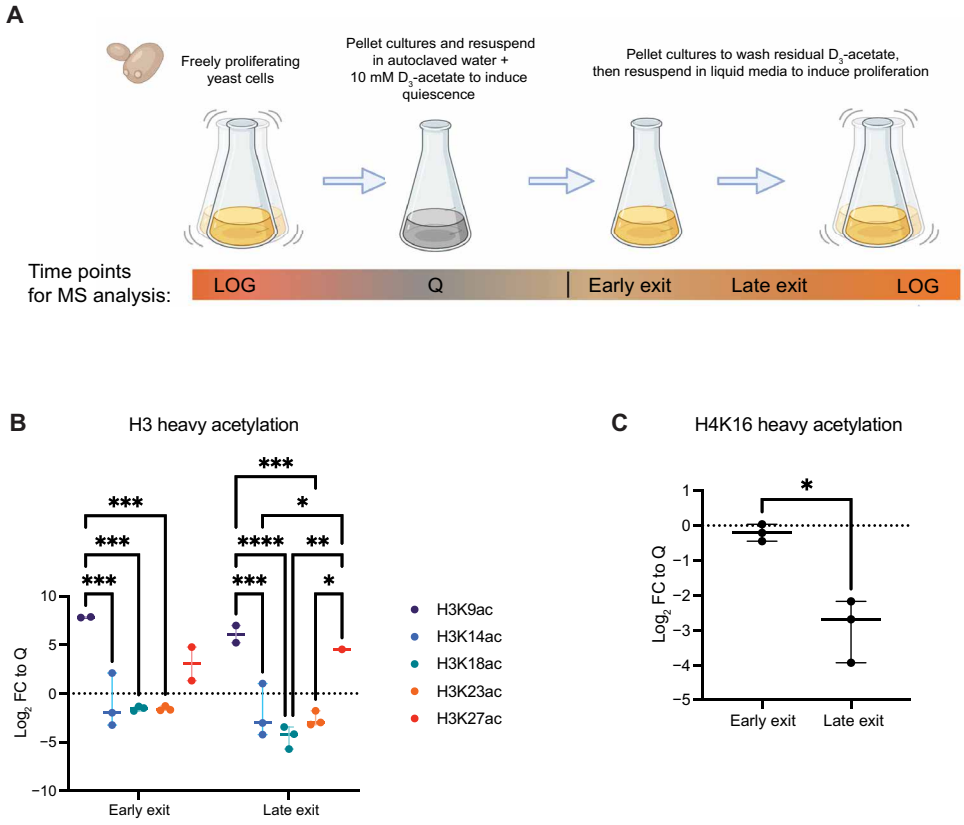

Fig. 2. Acetyl groups are transferred between histone lysine residues during yeast quiescent exit. (**A**) Experimental design for d_3-acetate labeling during yeast quiescence. (**B**) Heavy acetylation detected on histone H3 residues. Specific histone residues (K14, K18, and K23) have higher incorporation of heavy acetate during quiescence, while K9 and K27 have higher incorporation of heavy acetate during quiescent exit, at both early and late time points. *P* values were calculated using two-way ANOVA with Sidak's multiple comparisons test. *$P_{adj} < 0.05$, **$P_{adj} < 0.01$, ***$P_{adj} < 0.001$, and ****$P_{adj} < 0.0001$. (**C**) Heavy acetylation detected for H4K16 site, showing more enriched incorporation of heavy acetate during quiescence. *P* value was calculated using unpaired *t* test. *$P = 0.0282$.

Overall, our results suggest a direct transfer of intact acetate between histone residues during yeast quiescence exit. To further demonstrate that d_3-acetate is derived from histone acetylation during quiescence exit, we used a targeted MS approach to detect and quantify d_3-acetate in yeast cells. We induced proliferation by adding glucose-rich medium in the presence of HDAC inhibitors (HDACi) trichostatin A (TSA) and nicotinamide, predicting that the inhibitors would prevent release of d_3-acetate from histones during quiescence exit. We detected a spike of intracellular d_3-acetate during the early exit time points, which was not detected in the HDACi-treated cells (fig. S3B). This suggests that histone acetylation is the major source of d_3-acetate in cells exiting quiescence, further supporting our model of acetyl group transfer between histone lysine residues.

Chromatin-bound Acs2 is linked to transcriptional changes during quiescence exit

The yeast MS data indicated that acetyl groups can be transferred between lysine residues during quiescence exit. We next investigated whether ACSS2 is at a genomic location to facilitate this transfer. Similar to ACSS2 in mammalian cells (*12*, *14*), the yeast ortholog Acs2 translocates from the cytoplasm to the nucleus—in freely proliferating yeast, over 95% of Acs2 shows nuclear localization (*28*). Intriguingly, while mammalian ACSS2 is chromatin-bound in neurons (*12*) and other cell types (*14*), it remains unknown whether yeast Acs2 binds to chromatin.

To investigate whether Acs2 is recruited to chromatin in yeast, we performed chromatin immunoprecipitation coupled with high-throughput sequencing (ChIP-seq) using a previously validated mammalian ACSS2 antibody (*12*) that cross-binds to yeast Acs2 (fig. S4A) and, in parallel, an *S. cerevisiae* strain expressing endogenously tandem affinity purification (TAP)-tagged Acs2 (YLR153C; fig. S4B). Using both approaches, Acs2 was chromatin-bound and displayed similar patterns of enrichment during quiescence (Q), quiescence exit (early, 30 min or late, 240 min), and log proliferation (Fig. 3, A and B). Specifically, Acs2 peaks detected with the ACSS2 antibody (n = 1438) were induced during quiescence exit with highest enrichment in log proliferating cells (Fig. 3A, left). At the same genomic loci, TAP-tagged Acs2 showed strong enrichment in a similar pattern (Fig. 3A, right). Similarly, TAP-Acs2 peaks (n = 1284) were recruited throughout quiescence exit into log proliferation and showed a strong overlap with nontagged Acs2 enrichment at the same genomic loci (Fig. 3B). Chromatin recruitment and overlapping patterns of Acs2 and TAP-Acs2 enrichment were also observed during quiescence and early quiescence exit, although the number of peaks was markedly lower in these states (148 Acs2 peaks in quiescence, 119 Acs2 peaks in E30, and 763 Acs2 peaks in E240) (fig. S5, A to C). Gene ontology (GO)

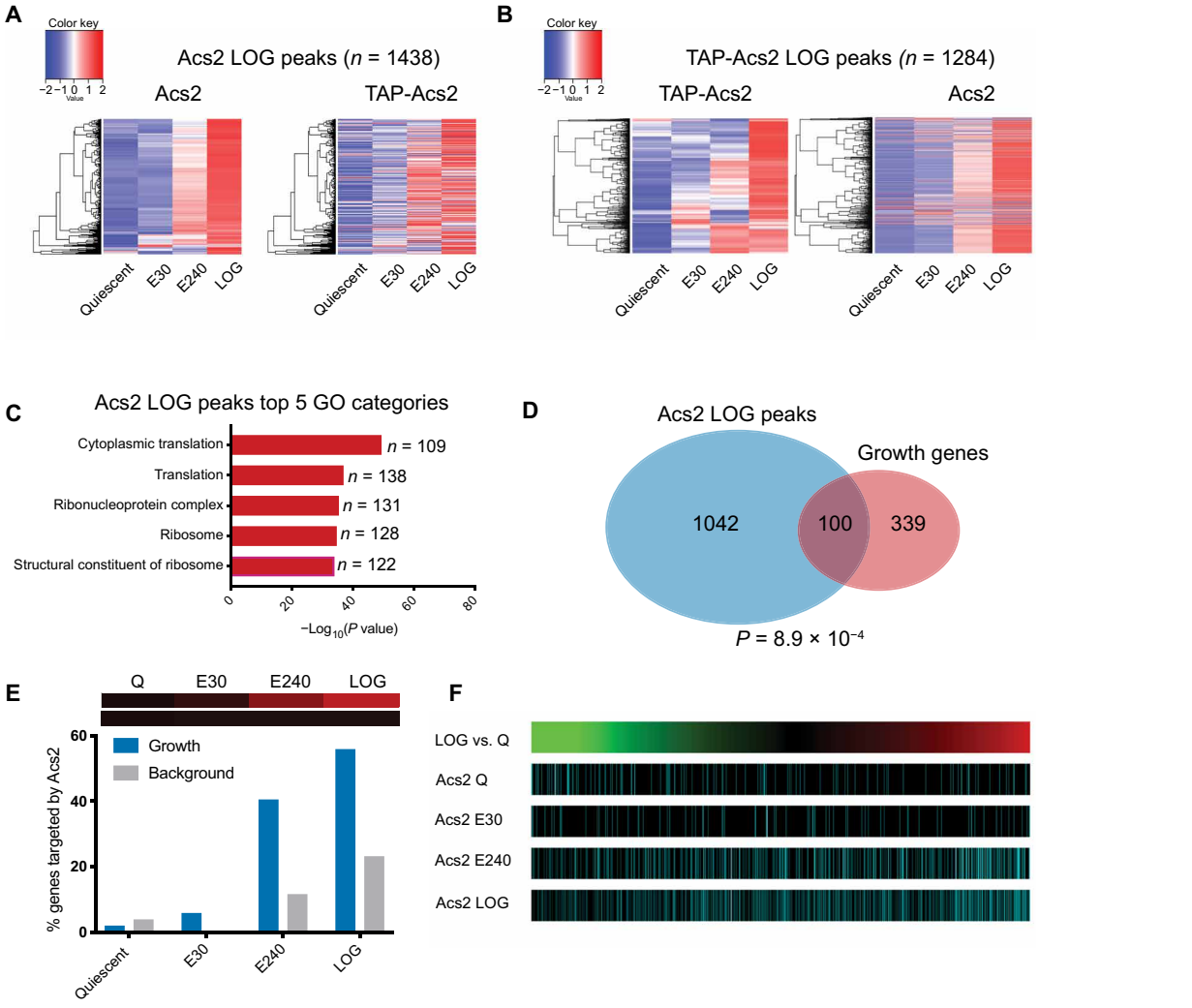

Fig. 3. Chromatin-bound Acs2 regulates gene expression in *S. cerevisiae*. (**A** and **B**) Acs2 is increasingly recruited to chromatin during cell proliferation. Endogenous untagged and TAP-tagged Acs2 peaks called in LOG proliferating *S. cerevisiae* show considerable overlap throughout quiescence exit. (A) Heatmaps ranked by endogenous Acs2 peaks. (B) Heatmaps ranked by TAP-tagged Acs2 peaks. (**C**) Gene ontology analysis of Acs2 LOG peaks. Top 5 most enriched categories and number of genes in each are shown. (**D**) Venn diagram showing significant overlap ($n = 100$; $P = 8.9 \times 10^{-4}$, hypergeometric test) of Acs2 LOG peaks ($n = 1142$) and annotated growth genes ($n = 439$). (**E**) Acs2 is preferentially recruited to growth genes that show increased expression during quiescence exit ($n = 52$) compared to background genes. Gradient bars represent gene expression changes and bar graphs show the percentage of genes targeted by Acs2 throughout the time course at growth genes and an equal number of randomly selected background genes. (**F**) Acs2 is preferentially recruited to the most up-regulated genes. Gradient bar ranked by gene expression changes during quiescence exit. Genes with the largest expression changes (LOG/Q) are on the right side (red), while the genes with smallest expression changes are on the left side (green). Acs2 peaks called in specific states (Q, E30, E240, and LOG) are shown below in cyan bars.

analysis of Acs2 peaks in log proliferating cells revealed significant enrichment near genes of cytoplasmic translation ($n = 109$ genes, $P = 3.9 \times 10^{-50}$), translation ($n = 138$ genes, $P = 1.27 \times 10^{-37}$), and ribosome components ($n = 128$ genes, $P = 2.06 \times 10^{-35}$) (Fig. 3C). We observed similar GO categories in quiescent and quiescence-exiting cells (fig. S6, A to C), suggesting that chromatin-bound Acs2 is particularly important for regulating the expression of genes related to cell growth and proliferation. Further, Acs2 peaks in log proliferating cells ($n = 100$ overlapping peaks, $P = 8.9 \times 10^{-4}$ from hypergeometric test; Fig. 3D) as well as in quiescent and quiescence-exiting cells (fig. S7, A to C) overlapped significantly with annotated growth genes from the literature (table S1).

We next investigated the relationship between Acs2 recruitment and gene expression. Notably, growth genes induced through each consecutive stage of quiescence exit ($n = 52$) were significantly more likely to be targeted by Acs2 than an equal number of background genes with no transcriptional changes ($P < 0.001$, Monte Carlo simulation; Fig. 3E). Similarly, a larger proportion of growth genes with increased expression in log proliferating versus quiescent cells ($n = 392$ of the 439 annotated growth genes) were targeted by Acs2 compared to background genes ($P < 0.001$, Monte Carlo simulation; fig. S8). Overall, Acs2 preferentially targeted genes with the largest transcriptional changes during quiescence exit, especially at E240 and LOG (Fig. 3F). Together, these results link chromatin-bound

Acs2 to transcriptional regulation during yeast quiescence exit, particularly for genes related to growth and cell proliferation.

Histone marks show distinct acetylation patterns during yeast quiescent exit

Our in vivo heavy labeling results outlined distinct patterns of deuterated acetate incorporation, and we observed transfer of intact acetate between lysine residues during quiescence exit (Fig. 2). To further investigate this relationship, we examined site-specific changes in endogenous (light) acetylation during quiescence exit both globally and specifically at genomic regions proximal to Acs2 binding. We profiled global histone acetylation levels via MS and ChIP-seq to investigate acetylation dynamics during the change of state. For all lysine residues of histone H3, there was increasing MS enrichment during quiescence exit (Fig. 4A), which is consistent with previous reports of increased histone acetylation upon re-feeding with glucose (*24*, *25*). Intriguingly, however, we observed marked differences in the behavior of specific lysine residues: Acetylation of certain sites (K9 and K27) was negligible during quiescence and strongly induced upon exit, while acetylation of others (K14, K18, and K23) was more stable across different states (Fig. 4A). Notably, these distinct patterns overlapped with the distinct behavior of these marks in the in vivo transfer experiment (Fig. 2), which could indicate a previously unappreciated divergence in the functional role of specific lysine residues. Lowly abundant histone acetylation marks tended to show more dynamic changes during quiescence exit (Fig. 4) and acted as acceptors of acetyl groups (Fig. 2), suggesting a close relationship with transcriptional up-regulation. On the other hand, highly abundant acetyl marks tended to be less dynamic (Fig. 4) and primarily acted as donors of heavy-labeled acetyl groups during quiescence exit (Fig. 2), indicating a potential role as primary reservoirs of acetyl groups. We also observed induction of H4K16ac during early and late exit (Fig. 4B), and the fold change of K16ac enrichment was similar to those of H3K14ac, K18ac, and K23ac.

To investigate acetylation dynamics using a parallel approach, we performed ChIP-seq using antibodies specific to the acetylated form of different lysine residues. Specifically, we examined the behavior of H3K9ac, H3K18ac, H3K23ac, and H3K27ac peaks during quiescence exit genome-wide. In line with the MS data, H3K18ac and H3K23ac peaks observed in quiescence decreased during cell proliferation, while H3K9ac and H3K27ac log peaks were increased (Fig. 4C, top). In addition, H3K9ac and H3K27ac gains showed a strong overlap with Acs2 recruitment to chromatin (Fig. 4C, bottom), suggesting that local, chromatin-bound Acs2 might facilitate the deposition of acetyl groups at these residues.

To further assess the effect of Acs2 recruitment on local histone acetylation changes, we examined H3K9ac, H3K18ac, H3K23ac, and H3K27ac enrichment in the vicinity of Acs2 peaks recruited during quiescence exit. Remarkably, during quiescence exit within 1 kb of Acs2 peaks, the enrichment of H3K18ac and H3K23ac decreased, while the enrichment of H3K9ac and H3K27ac increased ($P < 0.0001$, permutation test) (Fig. 4D). For example, Acs2 was recruited to the *Shr3* gene during quiescence exit, a gene that encodes an integral endoplasmic reticulum protein, and whose transcription was induced in proliferating cells with increased H3K9ac and decreased H3K18ac (fig. S9A), suggesting potential local acetyl group transfer. Similar patterns of Acs2 recruitment, increased H3K9ac, decreased H3K18ac, and increased gene expression were observed at numerous other genes, including *Yrb1*, encoding a protein involved in nuclear RNA export (fig. S9B), and *Pre9*, encoding a subunit of the 20*S* proteasome (fig. S9C).

Together, these results suggest that different histone lysine residues exhibit distinct acetylation patterns during quiescence exit. Certain lysines appear to function as "reservoir" sites that can act as nuclear stores of acetate during quiescence, while other sites mainly function as "activating" sites that receive acetyl groups to mediate rapid transcriptional activation during quiescence exit (Fig. 4E). These acetylation changes are facilitated by locally bound Acs2 that converts acetate into acetyl-CoA for re-incorporation.

DISCUSSION

Our in vitro and in vivo findings show that intact acetate can be directly transferred between histone acetyl-lysine residues. Using stable isotope labeling–based MS, we demonstrate in vitro that acetyl-CoA can be produced by ACSS2 from intact acetate released from a histone peptide by HDAC1, and this acetyl-CoA can subsequently be used by CBP to re-acetylate the histone peptide at a distinct site (Fig. 1). Notably, three purified mammalian enzymes (an HDAC, ACSS2, and a HAT) were sufficient to drive acetate transfer in vitro (Fig. 1). Emphasizing the critical role of each of the three essential enzymes in facilitating the transfer, we only detected significant transfer when all were present. Our in vitro work is, to our knowledge, the first to empirically demonstrate that intact acetate released from histones via HDAC activity can be directly converted to acetyl-CoA and used for histone acetylation. Previous studies have proposed the possibility of acetate recycling in cancers where ACSS2 is highly expressed in the nucleus. In glioblastoma cells, ACSS2 translocates to the nucleus during glucose deprivation (*14*) and produces acetyl-CoA that is incorporated into histone acetylation at promoters of transcription factor EB target genes, thereby increasing expression of lysosomal and autophagy genes. Intriguingly, treatment with HDACi TSA led to a decrease in both nuclear acetyl-CoA levels and histone acetylation (using a pan-acetyl H3 antibody) at promoter regions of lysosomal genes (*13*, *14*). In our model, these unexpected observations are potentially explained by decreased availability of acetate following HDAC inhibition, which impedes acetyl-CoA production and histone acetylation.

ACSS2 has a well-established role in the cytoplasm, where it activates exogenous acetate to produce acetyl-CoA for lipid biosynthesis (*29*). Several studies have identified nuclear localization of ACSS2, in both mammalian (*12*, *30*) and yeast (*28*) model systems, and have highlighted ACSS2's role in maintaining nuclear acetyl-CoA pools for histone acetylation. In a recent study, mouse embryonic fibroblasts that contain inactivating mutations in both ACSS2 alleles ($ACSS2^{-/-}$) had a substantial decrease in ^{14}C-acetate incorporation into lipids and histones (*30*). In addition, these mice experienced reduced tumor growth, compared to $ACSS2^{+/+}$ mice. The important role of nuclear ACSS2 has been demonstrated in the context of learning and memory. Nuclear localization of ACSS2 increases during neuronal differentiation in a cell line model and in primary mouse hippocampal neurons, which is accompanied with ACSS2 chromatin recruitment, enrichment of histone acetylation, and transcriptional activation of neuronal genes (*12*). Further, reduction of ACSS2 in mouse dorsal hippocampus impaired long-term memory formation (*12*). A common theme in these studies is metabolic alteration in the system, which underscores an importance of ACSS2 as a key epigenetic regulator during metabolic stress. Here, our findings indicate that

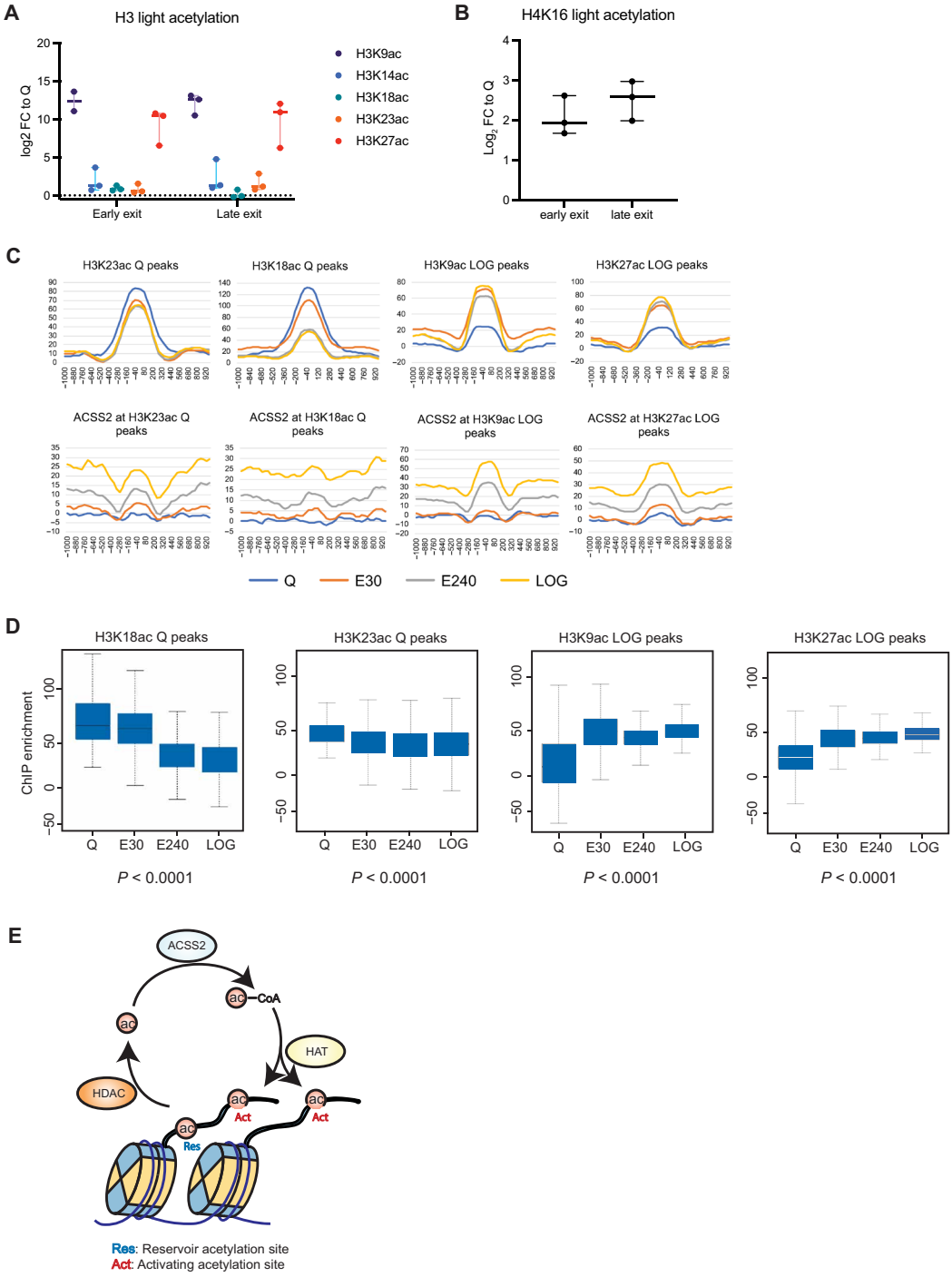

Fig. 4. Dynamic changes in histone acetylation during yeast quiescence exit. (**A**) Light acetylation detected for histone H3 residues. Global acetylation increases during quiescence exit, but K9ac and K27ac induction is higher compared to H3K14/18/23. (**B**) Light acetylation detected for H4K16ac, showing that acetylation increases during quiescence exit, at a fold change similar to K14/18/23 residues. (**C**) Metaplots showing H3K18ac, H3K23ac, H3K9ac, and H3K27ac 1 kb away from Acs2 Q to LOG gained peaks, and its Acs2 recruitment in quiescent, quiescence-exiting, and log proliferating cells. (**D**) Enrichment of H3K18ac Q peaks, H3K23ac Q peaks, H3K9ac LOG peaks, and H3K27ac LOG peaks within 1 kb of Acs2 gains during quiescence exit. *P* values ($P < 0.0001$) were calculated using permutation test. (**E**) Proposed model on the mechanism of ACSS2 in mediating local transfer of acetyl groups in chromatin from reservoir acetylation sites to activating acetylation sites.

during metabolic changes and especially in conditions with limited nutrient availability in yeast, nuclear ACSS2 can use acetate stores from histones to produce acetyl-CoA, which is then incorporated by HATs for histone acetylation and rapid transcriptional up-regulation. This outlines a novel mechanistic role for ACSS2 in the metabolic-epigenetic axis and invokes a reservoir function of histones, an emerging concept proposed by recent reviews (*10*, *31*). Moreover, this hypothesis is similar to the notion of metabolic channeling,

wherein substrates or metabolites are directed between enzymes in close proximity or as part of multiprotein complexes (*32*). While contested by some groups (*33*, *34*), others suggest that reaction rates could be increased by bringing enzymes close to each other, rather than having them distributed throughout the cell (*35*). On the basis of our in vitro and in vivo findings, we postulate that acetate could potentially be channeled by HDAC(s), ACSS2, and HAT(s) to mediate local histone acetylation and rapid gene activation.

Acs2 in yeast has also been characterized as a nuclear metabolic enzyme important for histone acetylation and gene activation. Studies using a temperature-sensitive Acs2 strain show decrease in histone acetylation compared to the wild-type strain (*28*). While it has been reported that Acs2 is nuclear in yeast, our findings further reveal that Acs2 is bound to chromatin (Fig. 3). By performing ChIP-seq using a commercially available ACSS2 antibody (that cross-reacts to yeast Acs2) and an endogenously TAP-tagged Acs2 strain, we observed Acs2 recruitment to chromatin during quiescence, quiescence exit, and log proliferation (Fig. 3). We found that induced growth genes during quiescence exit were preferentially targeted by Acs2, suggesting that Acs2 is recruited at these regions to produce acetyl-CoA and promote gene expression (Fig. 3). Acs2 recruitment overlapped with increased enrichment of H3K9ac and H3K27ac (Fig. 4C). Also consistent with previous reports (*24*), our MS analysis showed increased global histone acetylation during quiescence exit, particularly at H3K9 and H3K27. In addition, stable isotope labeling experiments using d_3-acetate indicated that these sites are highly enriched with heavy acetate labeling during quiescence exit (Fig. 2), suggesting that intact acetyl groups were transferred from neighboring sites that initially stored heavy acetate during quiescence. A previous study in yeast demonstrated that acetylation at specific lysine residues such as H3K9 and H3K27 is highly induced upon quiescence exit through Gcn5 acetyltransferase activity (*24*), which is consistent with our findings.

Our study indicates the importance of histones as reservoirs for acetyl groups, which can be rapidly mobilized for histone acetylation and transcriptional activation. Notably, we observed that there are different patterns of acetylation changes occurring during quiescence exit, wherein some sites are more highly induced than others upon exit. Thus, we hypothesize that specific lysine residues can function as reservoir acetylation sites to serve as local stores for acetyl groups (Fig. 4E). Then, acetate is released and transferred to activating acetylation sites when cells exit quiescence and transcriptional demand increases. Although we propose histones as reservoirs for acetyl groups, several nuclear nonhistone proteins are also HDAC substrates. For instance, HDAC1 interacts with and deacetylates the tumor suppressor protein p53, leading to p53 degradation (*36*). Several lysine acetyltransferases, such as p300, are also dynamically acetylated and deacetylated (*37*). However, considering their nuclear stoichiometry, histones are likely the most important source with strongest influence on gene regulation. Histone proteins are highly abundant in the nucleus and thus can store substantial amounts of acetate (*10*). Moreover, our in vivo experiments show that HDACi treatment prevents the release of d_3-acetate during quiescence exit (fig. S3B), further corroborating the likely role of histones as acetyl group reservoirs.

While we demonstrate this acetyl transfer in yeast quiescence exit as a change-of-state model, future studies will address these mechanisms in mammalian change-of-state models such as neuronal differentiation or in disease models such as cancer, wherein some tumors are more preferentially dependent on acetate for growth (*30*). It remains to be determined whether a local transfer of acetyl groups occurs when these cells undergo metabolic stress, which could then drive the expression of genes essential for survival. In addition, further studies will be necessary to interrogate the spatial constraints of local acetyl-CoA production by ACSS2. This question is particularly important in light of recent studies highlighting the importance of phase-separated domains in chromatin for transcriptional activation (*38*, *39*). Coactivator proteins such as MED1 and BRD4 have been found to associate in phase-separated condensates to drive gene expression (*40*). It is possible that an increased local acetyl-CoA pool is generated at these domains though ACSS2 activity, which is important for maintaining histone acetylation and gene activation.

In summary, our findings reveal direct transfer of intact acetate between histone acetyl-lysine residues, by coordinated activity of epigenetic and metabolic enzymes. These novel mechanisms may be critical to maintain proper epigenetic and transcriptional regulation during changes in metabolic states of the cell.

MATERIALS AND METHODS

Sample preparation for in vitro peptide reactions

Synthetic histone peptides corresponding to the first 42 amino acids of the histone H3.1 tail were purchased from New England Peptide. In vitro reactions were performed by incubating 20 μM synthetic peptide with 500 nM ACSS2, 1.5 μM HDAC1, 70 nM CBP, 20 μM ATP, and 100 μM CoA for 2 hours at 37°C. The reaction buffer consists of 150 mM NaCl, 50 mM Hepes (pH 7.5), and 1 mM $MgCl_2$. After incubation, samples were prepared for either acetyl-CoA or peptide analysis.

For acetyl-CoA analysis, the samples were quenched by adding acetonitrile + 0.6% formic acid (FA) solution. The samples were vortexed, and 100% methanol was added in excess to precipitate proteins in the sample. Then, the samples were centrifuged for 3400*g* for 5 min at room temperature, and the supernatant was transferred to a new tube, making sure the pipette tip does not touch the pellet. The samples were dried in the SpeedVac. Once ready to inject in the MS, the samples were reconstituted in buffer A (10 mM ammonium bicarbonate, pH 9.50).

For peptide analysis, the reactions were quenched by adding 0.1% trifluoroacetic acid. The pH of all the samples was checked to make sure that all samples were acidic (pH < 2). Samples were desalted using C_{18} stage tips and eluted in 40% acetonitrile in 0.1% FA. The 40% acetonitrile elution was optimized such that only the intact synthetic histone peptide was eluted from the C_{18} stage tip, and not the other proteins in the reaction mixture. The samples were then dried in the SpeedVac. Once ready to inject in the MS, the samples were reconstituted in 0.1% FA. To verify the newly labeled peptide, the samples containing the intact synthetic peptide (after C18 stage tipping) were subjected to derivatization, trypsin digestion, and bottom-up histone peptide analysis, using the same protocol for acid-extracted histones mentioned below.

Acetyl-CoA analysis via single reaction monitoring

Samples were injected onto an Acquity UPLC BEH C18 column (1.7-μm particle size, 2.1 mm by 50 mm, Waters) using a Vanquish UHPLC (ultrahigh-performance liquid chromatography) system (Thermo Fisher Scientific, San Jose, CA, USA). The HPLC pumped a constant flow rate of 0.4 ml/min with a programmed gradient

from 0.1 to 20% solvent B (100% acetonitrile) for 1.75 min, followed by a gradient from 20 to 95% over 0.10 min, and then isocratic flow at 95% for 6 min. The UHPLC was coupled online with TSQ Altis Triple Quadrupole Mass Spectrometer (Thermo Fisher Scientific) acquiring data in a single reaction monitoring mode. Q1 and Q3 resolution was set to 0.7 full width at half maximum and collision gas pressure at 1.5 mtorr. The precursor and product *m*/*z* targeted are as follows: 810.130 and 303.140 for light (^{12}C) acetyl-CoA, and 813.100 and 306.100 for heavy (^{2}H) acetyl-CoA at a collision energy of 35 V. The SRM data obtained were analyzed via Skyline, wherein the peak areas corresponding to 306.100 *m*/*z* were extracted for each sample, which corresponds to the intensity of the heavy acetyl-CoA fragment.

Peptide analysis via PRM

Samples were injected onto a 75 μm inside diameter (ID) × 25 cm Reprosil-Pur C18-AQ (3 μm; Dr. Maisch GmbH, Germany) nanocolumn packed in-house using an EASY-nLC nanoHPLC (Thermo Fisher Scientific, San Jose, CA, USA). The nanoLC pumped a flow rate of 300 nl/min, with a programmed gradient from 5 to 28% solvent B (A = 0.1% FA; B = 80% acetonitrile, 0.1% FA) over 45 min, followed by a gradient from 28 to 80% solvent B in 5- and 10-min isocratic at 80% B. The instrument was coupled online with an Orbitrap Fusion (Thermo Fisher Scientific, San Jose, CA, USA) mass spectrometer acquiring data in a targeted MSn method. The mass range was set to 100 to 1000 *m*/*z* with 54-ms maximum injection time and automatic gain control (AGC) target of 50,000. MS/MS was performed using electron transfer dissociation (ETD) fragmentation, with an ETD reaction time of 20 ms and ETD reagent target of 100,000. The data were acquired in the Orbitrap with a resolution of 30,000. A mass list table was added where *m*/*z* of the unmodified and acetylated forms of the synthetic peptide at a charge state of +9 was added. The following *m*/*z* values were added in the mass list table: 518.6433 (3 ac*), 508.6362 (1 ac*), 503.6326 (unmodified), 513.6398 (2 ac*), 508.3005 (1 ac), 513.304 (1 ac* 1 ac), 517.9719 (1 ac* 2 ac), and 512.9683 (2 ac). A charge state of +9 was used since it is the most intense charge state that the peptide exists in. With the PRM method, the instrument only targets the specified precursor *m*/*z* for fragmentation (*41*). The PRM data obtained were searched using Byonic and quantified both manually and via Skyline. Byonic was used to identify the modifications present in each sample and to identify the site-localizing fragments used for quantification. The data were analyzed manually and through Skyline, wherein three site-localizing fragment ions were summed to obtain the intensity of the modified peptide.

Histone extraction, propionylation, and digestion

Histones were extracted by using nuclei isolation buffer (NIB) as previously described (*21*). The cells were incubated in NIB [15 mM tris-HCl, 15 mM NaCl, 60 mM KCl, 5 mM $MgCl_2$, 1 mM $CaCl_2$, and 250 mM sucrose at pH 7.5; 0.5 mM 4-(2-aminoethyl)benzenesulfonyl fluoride hydrochloride (AEBSF), 10 mM sodium butyrate, 5 μM microcystin, and 1 mM dithiothreitol (DTT) added fresh] with 0.2% NP-40 on ice for 5 min. Two rounds of NIB incubation were performed at a volume buffer:cell pellet of 10:1: the first round with 0.2% NP-40 added to lyse the cell membrane, and the second without NP-40 to remove the detergent from the nuclear pellet. Each step included centrifugation at 700*g* for 5 min to pellet the intact nuclei. Next, the pellet was incubated in 0.2 M H_2SO_4 for 2 hours, and the supernatant was collected after centrifugation for 5 min at 3400*g*. Last, histones were precipitated with 33% trichloroacetic acid (TCA) overnight. The histone pellet was then washed with ice-cold acetone to remove residual TCA.

Histones were derivatized and digested as previously described (*21*). Histone pellets were resuspended in 20 μl of 50 mM ammonium bicarbonate (pH 8.0), and 10 μl of derivatization mix was added to the samples, which consist of propionic anhydride and acetonitrile in a 1:3 ratio (v/v), and this was immediately followed by the addition of 5 μl of ammonium hydroxide to maintain pH 8.0. The sample was incubated for 15 min at 37°C and dried, and the derivatization procedure was repeated one more time to ensure complete derivatization of unmodified and monomethylated lysine residues. Samples were then resuspended in 50 μl of 50 mM ammonium bicarbonate and incubated with trypsin (enzyme:sample ratio of 1:20) overnight at room temperature. After digestion, the derivatization reaction was performed again twice to derivatize the N termini of the peptides. Samples were desalted using C_{18} stage tips before LC-MS analysis.

Nano–LC-MS/MS for bottom-up histone peptide analysis

Samples were resuspended in 0.1% FA and injected onto a 75 μm ID × 25 cm Reprosil-Pur C18-AQ (3 μm; Dr. Maisch GmbH, Germany) nanocolumn packed in-house using an EASY-nLC nanoHPLC (Thermo Fisher Scientific, San Jose, CA, USA). The nanoLC pumped a flow rate of 300 nl/min with a programmed gradient from 5 to 28% solvent B (A = 0.1% FA; B = 80% acetonitrile, 0.1% FA) over 45 min, followed by a gradient from 28 to 80% solvent B in 5- and 10-min isocratic at 80% B. The instrument was coupled online with a Q-Exactive (Thermo Fisher Scientific, Bremen, Germany) mass spectrometer acquiring data in a DIA mode as previously optimized (*22*, *23*). Specifically, DIA consisted of a full-scan MS spectrum (*m*/*z* 300 to 1100) followed by 16 MS/MS with windows of 50 *m*/*z* and detected all in high resolution. The full-scan MS was acquired with a resolution of 35,000 and an AGC target of 2×10^5. MS/MS was performed with and AGC target of 2×10^5 using higher-collision dissociation with normalized collision energy of 27.

DIA data obtained from the bottom-up analysis were searched using EpiProfile 2.0 (*26*) and validated manually in Xcalibur (Thermo Fisher Scientific, Bremen, Germany). The peptide relative ratio was calculated using the total area under the extracted ion chromatograms of all peptides with the same amino acid sequence (including all of its modified forms) as 100%. For isobaric peptides, the relative ratio of two isobaric forms was estimated by averaging the ratio for each fragment ion with different mass between the two species. To obtain the % of heavy labeling for the yeast experiments, we used the intensity of the heavy-labeled form and divided by the sum of the total intensities of heavy and light peptides within the same amino acid sequence.

Yeast cultures and proteomics

Wild-type and endogenously TAP-tagged (YLR153C from Dharmacon, Horizon Discovery) *S. cerevisiae* glycerol stocks were streaked onto 2% agar plates containing yeast nitrogen base (Difco, #233520), synthetic complete amino acids mix (Bufferad, #S0051), and 2% glucose. Following overnight incubation at 30°C, starter cultures were inoculated with single colonies and incubated overnight at 30°C. Secondary cultures were inoculated at OD_{600} (optical density at 600 nm) = 0.2 and grown at 30°C until they reached OD_{600} = 1. Proliferating cultures were pelleted and resuspended in autoclaved water containing 10 mM d_3-acetate (Sigma-Aldrich, 176079) to induce quiescence. After 7 days, quiescent cultures were pelleted and washed

to remove any residual d_3-acetate, and proliferation was induced by resuspending in liquid medium. For preparing yeast cultures for d_3-acetate analysis, TSA and nicotinamide (dissolved in dimethyl sulfoxide) were added to liquid medium during proliferation for final concentrations of 25 μM and 5 mM, respectively, as has been used in the literature (*42*, *43*).

For proteomic analysis, yeast cultures were centrifuged and resuspended in buffer T [100 mM tris-HCl (pH 9.4) and 10 mM DTT] containing phenylmethylsulfonyl fluoride (PMSF) and 100 mM Na-butyrate. Cells were incubated at 30°C for 15 min, pelleted, and resuspended in buffer S [1.2 M sorbitol and 20 mM Na-Hepes (pH 7.4)] containing PMSF and 100 mM Na-butyrate. Cell walls were lysed using 50 U of Zymolyase 100T at 30°C for 15 min. Spheroplasting was confirmed under a light microscope by mixing cell lysate with equal volume of 1% SDS. When 80% spheroplasting was reached, lysis was stopped by the addition of 2× volume ice-cold buffer SM (2 M sorbitol, 20 mM Na-Hepes, and 1 mM $MgCl_2$) containing PMSF and 100 mM Na-butyrate. Subsequent cell lysis was performed using NIB buffer as described above.

Chromatin immunoprecipitation followed by sequencing

For ChIP-seq analysis, cultures were cross-linked with 1% formaldehyde at room temperature for 10 min. Reaction was stopped by adding 135 mM glycine. Cultures were then pelleted, washed, and resuspended in FA lysis buffer containing protease/phosphatase inhibitors and 10 mM Na-butyrate. Cells were lysed using 0.5-mm zirconia/silica beads (RPI, #9834) in a Mini-Beadbeater high-energy cell disruptor (BioSpec) at 4°C, for six times at 60 s. Samples were cooled on ice for 2-min in-between beatings. Subsequently, lysates were sonicated for 20 min in BioRuptor (Diagenode), using high setting and 30-s ON/OFF cycles. Cell debris was removed by centrifugation at 10,000 relative centrifugal force (rcf) for 15 min at 4°C. Sonication efficiency was confirmed for each sample by running on 0.8% agarose gel. Equal aliquots of sonicated lysates were used per immunoprecipitation reaction with 5 μl of H3K9ac antibody (Active Motif, 39317), 5 μl of H3K14ac antibody (Active Motif, 39697), 5 μl of H3K18ac antibody (Active Motif, 39755), 4 μl of H3K23ac antibody (Millipore, 07-355), 5 μl of H3K27ac antibody (Abcam, ab4729), 5 μl of H4K12ac antibody (Abcam, ab46983), 5 μl of H4K16ac antibody (Millipore, 07-329), 5 μl of Acs2 antibody (Thermo Fisher Scientific, MA5-14810), or 8 μl of TAP antibody (Invitrogen, CAB1001) preconjugated to Protein G Dynabeads (Life Technologies). Ten percent of the chromatin was saved as input DNA. ChIP reactions were incubated overnight at 4°C with rotation and washed three times in wash buffer. Immunoprecipitated DNA was eluted from the beads, reverse cross-linked, and purified together with the input DNA. Exactly 20 ng of DNA (either ChIP or input) was used to construct sequencing libraries using a NEBNext Ultra II DNA library preparation kit for Illumina [New England Biolabs (NEB)]. Libraries were multiplexed using NEBNext Multiplex Oligos for Illumina (dual index primers) and single-end sequenced [75 base pairs (bp)] on the NextSeq 550 platform (Illumina) in accordance with the manufacturer's protocol.

ChIP-seq analysis

ChIP-seq tags generated with the NextSeq 550 platform were demultiplexed using native applications on BaseSpace and aligned to the sacCer3 reference genome using Bowtie2 v2.3.4.1, (parameters --local -X 1000). Aligned tags were filtered for poor alignments using samtools v1.1 (samtools view -q 5 -bS) and merged over NextSeq lanes (samtools merge -n) and then filtered for polymerase chain reaction (PCR) duplicates using PICARD (java -jar picard.jar MarkDuplicates REMOVE_DUPLICATES = True ASSUME_SORT_ORDER = queryname). Peaks were detected using MACS2 (callpeak function, tag size = 75 bp; false discovery rate < 1×10^{-3} with genome size set to -g 12,157,105 and --nomodel set) from replicate-pooled histone acetylation PTM tags along with treatment-matched input tags as control. UCSC genome-browser track views were created for ChIP-seq data by first pooling replicates and generating coverage maps using BEDtools genomeCoverageBed -bg, and then adjusting for library size using the RPM (reads per million) coefficient. The input signal was then subtracted from the ChIP signal. The resulting tracks were converted from bedGraph to bigWig files using the bedGraphToBigWig utility in the UCSC Genome Browser. Proximity to ACSS2 peaks was assessed by expanding all ACSS2 peaks to 2 kb around the center and testing for overlap using bedtools intersect.

RNA sequencing

For RNA sequencing (RNA-seq), cultures were pelleted and resuspended in QIAzol (Qiagen). Cells were lysed using 0.5-mm zirconia/silica beads (RPI, #9834) in a Mini-Beadbeater high-energy cell disruptor (BioSpec) at 4°C, for four times at 60 s. Samples were cooled on ice for 2-min in-between beatings. RNA was subsequently purified using an RNeasy Mini kit (Qiagen). One microgram of RNA was used to construct sequencing libraries using a NEBNext Ultra II RNA library preparation kit for Illumina (NEB). Libraries were multiplexed using NEBNext Multiplex Oligos for Illumina (dual index primers) and single-end sequenced (75 bp) on the NextSeq 550 platform (Illumina) in accordance with the manufacturer's protocol.

RNA-seq analysis

All RNA-seq data were prepared for analysis as follows. NextSeq sequencing data were demultiplexed using native applications on BaseSpace. Demultiplexed FASTQs were aligned by RNA-STAR v.2.5.2 to the assembly sacCer3 (parameters --outFilterType BySJout --outFilterMultimapNmax 20 --alignSJoverhangMin 8 --alignSJDBoverhangMin 1 --outFilterMismatchNmax 999 --alignIntronMin 20 --alignIntronMax 1000000). Aligned reads were mapped to genomic features using HTSeq v.0.6.1 after merging lanes of NextSeq (parameters -r pos -s no -t exon -i gene_id). Quantification, library size adjustment, and analysis of differential gene expression were done using DESeq2 and Wald's test. Overlaps between lists of genes were tested for significance using a hypergeometric test [phyper() in R].

LC-MS quantitation of d_3-acetate

Aliquots (25 μl) of each thawed yeast pellet on ice were homogenized in 175 μl of 50:50 water/acetonitrile with 0.3% FA at 4°C using tough microorganism lysing tubes in a Precellys homogenizer (Bertin Corp., Rockville, MD). Wash and postwash medium samples were aliquoted and prepared without dilution. The input and prewash medium samples were diluted 1000× in deionized water before sample preparation. Then, d_3-acetate and d_3-lactate (internal standard) were derivatized in 50 μl of aliquots of yeast homogenate and medium with *O*-benzylhydroxylamine through a coupling reaction with 1-ethyl-3-(-3-dimethylaminopropyl) carbodiimide at room temperature for 10 min. This mixture was extracted with 600 μl of ethylacetate

with 50 μl of added deionized water followed by vortexing and centrifuging at 21,000*g* at 4°C. Aliquots of ethylacetate (50 μl) were dried under nitrogen at 30°C and reconstituted in 500 μl of 50% methanol in a 96-well plate. Derivatized d_3-acetate was quantitated by multiple reaction monitoring (d_3-acetate, *m/z* 169.1 to 91.1; d_3-lactate, *m/z* 199.1 to 91.1) with standard calibration curves on an Agilent 1290 Infinity UHPLC/6495B triple quadrupole mass spectrometer.

SUPPLEMENTARY MATERIALS

Supplementary material for this article is available at https://science.org/doi/10.1126/sciadv.abj5688

View/request a protocol for this paper from *Bio-protocol*.

REFERENCES AND NOTES

1. G. Egervari, K. M. Glastad, S. L. Berger, Food for thought. *Science* **370**, 660–662 (2020).
2. X. Li, G. Egervari, Y. Wang, S. L. Berger, Z. Lu, Regulation of chromatin and gene expression by metabolic enzymes and metabolites. *Nat. Rev. Mol. Cell Biol.* **19**, 563–578 (2018).
3. A. E. Boukouris, S. D. Zervopoulos, E. D. Michelakis, Metabolic enzymes moonlighting in the nucleus: Metabolic regulation of gene transcription. *Trends Biochem. Sci.* **41**, 712–730 (2016).
4. J. A. van der Knaap, C. P. Verrijzer, Undercover: Gene control by metabolites and metabolic enzymes. *Genes Dev.* **30**, 2345–2369 (2016).
5. J. P. Etchegaray, R. Mostoslavsky, Interplay between metabolism and epigenetics: A nuclear adaptation to environmental changes. *Mol. Cell* **62**, 695–711 (2016).
6. G. Figlia, P. Willnow, A. A. Teleman, Metabolites regulate cell signaling and growth via covalent modification of proteins. *Dev. Cell* **54**, 156–170 (2020).
7. A. J. Bannister, T. Kouzarides, Regulation of chromatin by histone modifications. *Cell Res.* **21**, 381–395 (2011).
8. S. Sivanand, I. Viney, K. E. Wellen, Spatiotemporal control of acetyl-CoA metabolism in chromatin regulation. *Trends Biochem. Sci.* **43**, 61–74 (2018).
9. P. Mews, G. Egervari, R. Nativio, S. Sidoli, G. Donahue, S. I. Lombroso, D. C. Alexander, S. L. Riesche, E. A. Heller, E. J. Nestler, B. A. Garcia, S. L. Berger, Alcohol metabolism contributes to brain histone acetylation. *Nature* **574**, 717–721 (2019).
10. C. Ye, B. P. Tu, Sink into the epigenome: Histones as repositories that influence cellular metabolism. *Trends Endocrinol. Metab.* **29**, 626–637 (2018).
11. V. Bulusu, S. Tumanov, E. Michalopoulou, N. J. van den Broek, G. MacKay, C. Nixon, S. Dhayade, Z. T. Schug, J. Vande Voorde, K. Blyth, E. Gottlieb, A. Vazquez, J. J. Kamphorst, Acetate recapturing by nuclear acetyl-CoA synthetase 2 prevents loss of histone acetylation during oxygen and serum limitation. *Cell Rep.* **18**, 647–658 (2017).
12. P. Mews, G. Donahue, A. M. Drake, V. Luczak, T. Abel, S. L. Berger, Acetyl-CoA synthetase regulates histone acetylation and hippocampal memory. *Nature* **546**, 381–386 (2017).
13. X. Li, X. Qian, Z. Lu, Local histone acetylation by ACSS2 promotes gene transcription for lysosomal biogenesis and autophagy. *Autophagy* **13**, 1790–1791 (2017).
14. X. Li, W. Yu, X. Qian, Y. Xia, Y. Zheng, J.-H. Lee, W. Li, J. Lyu, G. Rao, X. Zhang, C.-N. Qian, S. G. Rozen, T. Jiang, Z. Lu, Nucleus-translocated ACSS2 promotes gene transcription for lysosomal biogenesis and autophagy. *Mol. Cell* **66**, 684–697.e9 (2017).
15. M. Haberland, R. L. Montgomery, E. N. Olson, The many roles of histone deacetylases in development and physiology: Implications for disease and therapy. *Nat. Rev. Genet.* **10**, 32–42 (2009).
16. E. Seto, M. Yoshida, Erasers of histone acetylation: The histone deacetylase enzymes. *Cold Spring Harb. Perspect. Biol.* **6**, a018713 (2014).
17. C. A. Johnson, D. A. White, J. S. Lavender, L. P. O'Neill, B. M. Turner, Human class I histone deacetylase complexes show enhanced catalytic activity in the presence of ATP and co-immunoprecipitate with the ATP-dependent chaperone protein Hsp70. *J. Biol. Chem.* **277**, 9590–9597 (2002).
18. S. Sidoli, S. Trefely, B. A. Garcia, A. Carrer, Integrated analysis of acetyl-CoA and histone modification via mass spectrometry to investigate metabolically driven acetylation. *Methods Mol. Biol.* **1928**, 125–147 (2019).
19. M. J. Sweredoski, A. Moradian, S. Hess, High-resolution parallel reaction monitoring with electron transfer dissociation for middle-down proteomics: An application to study the quantitative changes induced by histone modifying enzyme inhibitors and activators. *Methods Mol. Biol.* **1647**, 61–69 (2017).
20. K. R. Karch, S. Sidoli, B. A. Garcia, Identification and quantification of histone PTMs using high-resolution mass spectrometry. *Methods Enzymol.* **574**, 3–29 (2016).
21. S. Sidoli, N. V. Bhanu, K. R. Karch, X. Wang, B. A. Garcia, Complete workflow for analysis of histone post-translational modifications using bottom-up mass spectrometry: From histone extraction to data analysis. *J. Vis. Exp.*, 54112 (2016).
22. S. Sidoli, S. Lin, L. Xiong, N. V. Bhanu, K. R. Karch, E. Johansen, C. Hunter, S. Mollah, B. A. Garcia, Sequential window acquisition of all theoretical mass spectra (SWATH) analysis for characterization and quantification of histone post-translational modifications. *Mol. Cell. Proteomics* **14**, 2420–2428 (2015).
23. S. Sidoli, J. Simithy, K. R. Karch, K. Kulej, B. A. Garcia, Low resolution data-independent acquisition in an LTQ-Orbitrap allows for simplified and fully untargeted analysis of histone modifications. *Anal. Chem.* **87**, 11448–11454 (2015).
24. R. M. Friis, B. P. Wu, S. N. Reinke, D. J. Hockman, B. D. Sykes, M. C. Schultz, A glycolytic burst drives glucose induction of global histone acetylation by picNuA4 and SAGA. *Nucleic Acids Res.* **37**, 3969–3980 (2009).
25. P. Mews, B. M. Zee, S. Liu, G. Donahue, B. A. Garcia, S. L. Berger, Histone methylation has dynamics distinct from those of histone acetylation in cell cycle reentry from quiescence. *Mol. Cell. Biol.* **34**, 3968–3980 (2014).
26. Z. F. Yuan, S. Sidoli, D. M. Marchione, J. Simithy, K. A. Janssen, M. R. Szurgot, B. A. Garcia, EpiProfile 2.0: A computational platform for processing epi-proteomics mass spectrometry data. *J. Proteome Res.* **17**, 2533–2541 (2018).
27. Z. F. Yuan, S. Lin, R. C. Molden, X. J. Cao, N. V. Bhanu, X. Wang, S. Sidoli, S. Liu, B. A. Garcia, EpiProfile quantifies histone peptides with modifications by extracting retention time and intensity in high-resolution mass spectra. *Mol. Cell. Proteomics* **14**, 1696–1707 (2015).
28. H. Takahashi, J. M. McCaffery, R. A. Irizarry, J. D. Boeke, Nucleocytosolic acetyl-coenzyme a synthetase is required for histone acetylation and global transcription. *Mol. Cell* **23**, 207–217 (2006).
29. A. Luong, V. C. Hannah, M. S. Brown, J. L. Goldstein, Molecular characterization of human acetyl-CoA synthetase, an enzyme regulated by sterol regulatory element-binding proteins. *J. Biol. Chem.* **275**, 26458–26466 (2000).
30. S. A. Comerford, Z. Huang, X. du, Y. Wang, L. Cai, A. K. Witkiewicz, H. Walters, M. N. Tantawy, A. Fu, H. C. Manning, J. D. Horton, R. E. Hammer, S. L. McKnight, B. P. Tu, Acetate dependence of tumors. *Cell* **159**, 1591–1602 (2014).
31. R. Boon, G. G. Silveira, R. Mostoslavsky, Nuclear metabolism and the regulation of the epigenome. *Nat. Metab.* **2**, 1190–1203 (2020).
32. L. J. Sweetlove, A. R. Fernie, The role of dynamic enzyme assemblies and substrate channelling in metabolic regulation. *Nat. Commun.* **9**, 2136 (2018).
33. B. M. Bakker, F. I. C. Mensonides, B. Teusink, P. van Hoek, P. A. M. Michels, H. V. Westerhoff, Compartmentation protects trypanosomes from the dangerous design of glycolysis. *Proc. Natl. Acad. Sci. U.S.A.* **97**, 2087–2092 (2000).
34. J. P. Dexter, P. S. Ward, T. Dasgupta, A. M. Hosios, J. Gunawardena, M. G. Vander Heiden, Lack of evidence for substrate channeling or flux between wildtype and mutant isocitrate dehydrogenase to produce the oncometabolite 2-hydroxyglutarate. *J. Biol. Chem.* **293**, 20051–20061 (2018).
35. L. Aguilar-Arnal, S. Ranjit, C. Stringari, R. Orozco-Solis, E. Gratton, P. Sassone-Corsi, Spatial dynamics of SIRT1 and the subnuclear distribution of NADH species. *Proc. Natl. Acad. Sci. U.S.A.* **113**, 12715–12720 (2016).
36. J. Luo, F. Su, D. Chen, A. Shiloh, W. Gu, Deacetylation of p53 modulates its effect on cell growth and apoptosis. *Nature* **408**, 377–381 (2000).
37. J. C. Black, A. Mosley, T. Kitada, M. Washburn, M. Carey, The SIRT2 deacetylase regulates autoacetylation of p300. *Mol. Cell* **32**, 449–455 (2008).
38. Y. Zhang, T. G. Kutateladze, Liquid-liquid phase separation is an intrinsic physicochemical property of chromatin. *Nat. Struct. Mol. Biol.* **26**, 1085–1086 (2019).
39. G. J. Narlikar, Phase-separation in chromatin organization. *J. Biosci.* **45**, (2020).
40. A. Boija, I. A. Klein, B. R. Sabari, A. Dall'Agnese, E. L. Coffey, A. V. Zamudio, C. H. Li, K. Shrinivas, J. C. Manteiga, N. M. Hannett, B. J. Abraham, L. K. Afeyan, Y. E. Guo, J. K. Rimel, C. B. Fant, J. Schuijers, T. I. Lee, D. J. Taatjes, R. A. Young, Transcription factors activate genes through the phase-separation capacity of their activation domains. *Cell* **175**, 1842–1855.e16 (2018).
41. M. J. Sweredoski, A. Moradian, M. Raedle, C. Franco, S. Hess, High resolution parallel reaction monitoring with electron transfer dissociation for middle-down proteomics. *Anal. Chem.* **87**, 8360–8366 (2015).
42. K. J. Bitterman, R. M. Anderson, H. Y. Cohen, M. Latorre-Esteves, D. A. Sinclair, Inhibition of silencing and accelerated aging by nicotinamide, a putative negative regulator of yeast Sir2 and human SIRT1. *J. Biol. Chem.* **277**, 45099–45107 (2002).
43. B. J. E. Martin, J. Brind'Amour, A. Kuzmin, K. N. Jensen, Z. C. Liu, M. Lorincz, L. A. J. Howe, Transcription shapes genome-wide histone acetylation patterns. *Nat. Commun.* **12**, 210 (2021).

Acknowledgments: We thank K. Tran and L. Luense for critical reading of the manuscript. We also thank C. Petucci and the Penn Metabolomics Core in the Cardiovascular Institute for providing measurements of d_3-acetate. **Funding:** This work was supported by NIH grants RO1AA027202, P01AG031862, R01CA078831, and R01AG055570 (S.L.B.), F31 CA247348-02 (M.M.), K99AA028577 (G.E.), P01CA196539 (B.A.G.), and T32 GM-07229 (D.C.A.) and Alzheimer's Association grant AARF-19-618159 (G.E.). We wish to acknowledge

the National Institute on Aging Intramural Research Program (NIA IRP), NIH, for resource support (ZIA AG000679 to P.S.). **Author contributions:** Conceptualization: S.L.B., B.A.G., M.M., G.E., and S.S. Methodology: S.L.B., B.A.G., M.M., G.E., S.S., and G.D. Investigation: M.M., G.E., S.S., and G.D. Supervision: S.L.B., G.E., and B.A.G. Writing—original draft: M.M. and G.E. Writing—review and editing: S.L.B., M.M., G.E., S.S., D.C.A., P.S., and B.A.G. **Competing interests:** The authors declare that they have no competing interests. **Data and materials availability:** All raw mass spectrometry data files have been uploaded onto Chorus (https://chorusproject.org/pages/index.html) under project number 1742. ChIP-seq and RNA-seq data are provided online at NCBI GEO, under series accession GSE189446. All other data needed to evaluate the conclusions in the paper are present in the paper and/or the Supplementary Materials.

Submitted 1 June 2021
Accepted 29 November 2021
Published 21 January 2022
10.1126/sciadv.abj5688